Applied Physics A (2023) 129:148
https://doi.org/10.1007/s00339-023-06438-y

Applied Physics A
Materials Science & Processing

RAPID COMMUNICATIONS

Electrochemical detection of dopamine using green and chemical synthesized CuO/PANI nanocomposite modified electrode

Seleke J. Mokole[1,2] · Ahmed Aliyu[3,4] · Omolola E. Fayemi[1,2]

Received: 5 January 2023 / Accepted: 17 January 2023 / Published online: 28 January 2023

Abstract

Copper oxide (CuO) nanoparticles were synthesized using the chemical and green method routes and doped with polyaniline (PANI) to form PANI/CuO_{ch} and PANI/CuO_{gr} nanocomposite. The microstructural properties of the nanocomposites were characterized by UV–Vis spectroscopy (UV), X-ray diffraction (XRD), Fourier transform infrared spectroscopy (FTIR), and scanning electron microscopy equipped with energy-dispersive X-ray spectroscopy (EDS) detector. The electrochemical behavior of the CuO_{ch}, CuO_{gr}, PANI/CuO_{ch}, and PANI/CuO_{gr} electrodes was investigated using cyclic voltammetry (CV), and square wave voltammetry (SWV), and the results showed an enhanced electrochemical catalytic activity toward dopamine (DA) on PANI/CuO_{gr} electrodes. SWV was conducted for the determination of DA with a linear range from 26 to 95 µM and a low limit of detection (LOD) of 8.22 µM. A comparison between the PANI/CuO_{ch} and PANI/CuO_{gr} electrodes and other modified electrodes toward detection of DA are comparable with the reported literature results.

Keywords Dopamine · CuO nanoparticle · PANI · Nanocomposites · Electroanalysis

1 Introduction

Dopamine (DA), a monoamine neurotransmitter (NT) plays an important role in the function of the renal, central nervous, and hormonal systems. The abnormal DA concentration serves as a key indicator for human health issues and is used to monitor different life-threatening diseases, such as Parkinson's, Alzheimer's, and Huntington's diseases [1–3]. The diagnosis of these diseases necessitates accurate measurements of DA in biological samples due to its low concentration in the brain and its action depends on the overall levels and short burst, which makes its determination a challenging task [4, 5]. Different techniques including capillary electrophoresis, high-performance liquid chromatography, and electrochemical techniques have been reportedly used in the determination of DA [1, 6, 7]. Among these techniques, the electrochemical process happens to be the most promising and reliable technique due to its wide selectivity, high sensitivity, low cost of operation, and excellent results reproducibility [1, 8]. However, the overlapped oxidation potential of DA with other biomolecules such as ascorbic acid (AA) and uric acid (UA) has hindered the electrochemical determination of DA. Therefore, this problem can be addressed by modifying an electrode with appropriate materials for an effective way to improve the electrode sensitivity and selectivity [9].

Many materials such as copper oxide (CuO), zinc oxide (ZnO), iron oxide (FeO), and titanium oxide (TiO_2) nanoparticles have been used in the modification of bare electrodes for enhancement in electrochemical properties [10]. Among them, the CuO nanoparticles attract more attention because of their high electrical conductivity, non-toxicity, chemical stability, low cost, good catalytic behavior, and simplicity in the synthesis method [11] which play a significant role in their applications in the field of electrochemistry. To date,

✉ Omolola E. Fayemi
Omolola.Fayemi@nwu.ac.za

1 Department of Chemistry, School of Physical and Chemical Sciences, Faculty of Natural and Agricultural Sciences, North-West University (Mafikeng Campus), Private Bag X2046, Mmabatho 2735, South Africa

2 Material Science Innovation and Modelling (MaSIM) Research Focus Area, Faculty of Natural and Agricultural Sciences, North West University (Mafikeng Campus), Private Bag X2046, Mmabatho 2735, South Africa

3 Department of Chemical Engineering, Federal University Wukari, Wukari, Nigeria

4 Department of Materials Engineering, India Institute of Science, Bangalore, India

several chemical and physical methods have been developed for the synthesis of CuO nanoparticles with different morphology, particle size, surface area, and crystallinity. However, considerable research has been conducted on the chemical synthesis of CuO with some downsides due to the high cost of chemicals and the formation of toxic by-products which makes the process very difficult to commercialize [12]. In contrast, much work was not focused on the green synthesis of CuO even though it has more advantages over the chemical synthesis methods such as cost-effectiveness, simplicity, and compatibility with pharmaceutical applications [12, 13]. This method also provides a unique opportunity because the plant extract in the green synthesis can act as both a reducing and stabilizing agent [13, 14].

Despite all these advantages of the green synthesis of CuO and its application in the field of electrochemistry, more research is needed on how to enhance the surface of CuO for electrochemical determination. One way of doing this is by incorporating or doping the CuO with polymers to form nanocomposites. Nanocomposites are mostly used as an alternative to overcome the drawbacks in the stoichiometry and elemental composition control of micro and monolithic composite. Therefore, in the present investigation, a CuO nanoparticle that was synthesized using the green synthesis route was doped with polyaniline (PANI) and for comparison purposes, CuO nanoparticles by chemical synthesis route were also doped with the PANI. PANI was chosen as a polymer in this study because of its high-temperature resistance, exceptional electrical conductivity, and reliable ecological stability [15].

The main aim of this study was to synthesize and compare the electrochemical behavior of CuO nanoparticles by chemical and green synthesis route doped with PANI (i.e., PANI/CuO_{ch} and PANI/CuO_{gr}) and further characterized to confirm their microstructural properties. Also, the determination of DA with the synthesized nanocomposite was attempted. To the best of our knowledge, this is the first report comparing the electrochemical detection of DA with electrodes composed of mainly PANI/CuO_{ch} and PANI/CuO_{gr} nanocomposite as the modifier.

2 Experimental section

2.1 Materials

Ziziphus mucronata dried leaves obtained from South Africa are used in the green synthesis of CuO. While Copper (II) nitrate trihydrate ($Cu(NO_3)_2.3H_2O$), dopamine hydrochloride, ethylene glycol, aniline hydrochloride, ammonium peroxydisulphate ($(NH_4)_2S_2O_8$), sodium hydroxide (NaOH), potassium ferrocyanide ($K_4[Fe(CN)_6]$), potassium ferricyanide ($K_3[Fe(CN)_6]$), hydrochloric acid, and N, N- dimethylformamide (C_3H_7NO) were purchased from Sigma-Aldrich (USA). All reagents were of analytical grade and used as received without any further purification. All solutions were prepared with deionized (DI), distilled water.

2.2 Green synthesis of copper oxide nanoparticles (CuO_{gr})

20 g of *Ziziphus mucronata* dried leaves were added to 100 mL of DI water in a 250 mL beaker and heated at 80 °C for 60 min. The dried leaves debris was separated from the yellow extract by filtration process and the filtrate was used for the CuO_{gr} NPs synthesis. 50 mL of the prepared leaves extract was added to 5 g of copper nitrate and the mixture was stirred at room temperature for 2 h. The resulting paste mixture was then transferred into a ceramic crucible and heated in a muffle furnace at 400 °C for 2 h. The resulting CuO_{gr} NPs are stored in an airtight container for further use.

2.3 Chemical synthesis of copper oxide nanoparticles (CuO_{ch})

The CuO_{ch} NPs were synthesized by dissolving 5 g of $Cu(NO_3)_2.3H_2O$ in 20 mL of ethylene glycol with constant stirring for 1 h at room temperature to obtain a homogeneous solution. The solution is kept for 24 h for gel formation. The final mixture was dried and calcinated at a temperature of 300°C in a muffle furnace for 1 h. The resulting product was then crushed to a fine powder and stored for further use.

2.4 Preparation of polyaniline (PANI)

2.59 g of aniline hydrochloride powder and 5.71 g of ammonium peroxydisulphate were dissolved in 50 mL distilled water in a volumetric flask with continuous stirring for 1 h at room temperature. The solution is kept for 24 h for polymerization. Then after, the polymerized mixture was filtered and the precipitate was collected and subsequently washed with 100 mL of 0.2 M HCl and 100 mL of acetone. Lastly, the resulting product is dried in an oven at 60 °C and stored for further use.

2.5 Preparation of PANI/CuO_{ch} and PANI/CuO_{gr} nanocomposites

10 mg of the prepared PANI was mixed with 10 mg of the synthesized CuO via a glass tube containing N, N- dimethylformamide. The mixture was sonicated at room temperature for 24 h. This process was performed for both the chemical and green synthesized CuO to form the corresponding PANI/CuO_{ch} and PANI/CuO_{gr} nanocomposite. Thereafter, the resulting PANI/CuO nanocomposite paste was stored for use and characterization.

2.6 Characterization

The synthesized materials (CuO_{ch}, CuO_{gr}, PANI/CuO_{ch}, and PANI/CuO_{gr} nanocomposites) were characterized using different spectroscopic and microscopic techniques. UV–Vis spectroscopy was carried out within a wavelength range of 200–700 using Uviline 94,000 UV spectrophotometer supplied by SI analytics, Germany. X-ray diffraction (XRD) patterns were recorded using Cu-Kα radiation ($\lambda = 0.1540$ nm) in Rontgen PW3040/60 X'Pert Pro X-ray diffractometer, in the 2θ range of 10°–90° with a scan rate of 2° min^{-1}. Fourier transform infrared spectroscopy (FTIR: Bruker Corporation, USA) (Opus Alpha-P) was used to determine the functional groups in the materials within a wavelength range of 400–4000 cm^{-1}. The scanning electron microscope (Quanta FEG 250, ThermoFisher Scientific, USA) equipped with energy-dispersive X-ray spectroscopy (EDS) detector was used to analyze the material's surface morphology and composition at 15 kV.

The cyclic voltammetry (CV) test was carried out in a probe solution of 5 nM $K_4[Fe(CN)_6]$ containing 0.1 M phosphate buffer saline (pH, 7.4) using a three-electrode workstation (Autolab potentiostat/galvanostat PGSAT-20 on Nova 1.3 software) to investigate the electrochemical redox response of the bare, CuO_{ch}, CuO_{gr}, PANI/CuO_{ch}, and PANI/CuO_{gr} nanocomposites. The nanocomposite was used as the working electrode, while platinum wire and standard Ag/AgCl electrodes were used as auxiliary and referenced electrodes, respectively. The redox response of PANI/CuO_{ch} and PANI/CuO_{gr} working electrodes used in the analytical procedures were further examined in detail using the same technique. The voltammograms were recorded in a potential scan from − 0.5 to 0.9 V, using a potential step size of 0.001 V.

3 Results and discussion

3.1 UV–Vis analysis

Figure 1 shows the UV–Vis absorption spectra obtained for CuO_{ch}, CuO_{gr}, PANI, PANI/CuO_{ch}, and PANI/CuO_{gr} nanocomposite. Figure 1a and b shows an absorbance peak at 290.5 nm and 289.5 nm for CuO_{ch} and CuO_{gr}, respectively. The peal appearance in the UV region can be attributed to the presence of very fine copper nanoclusters which gave rise to dipole moment oscillation [12, 16]. However, the UV spectra of the PANI in Fig. 1c show an absorbance peak at 294.8 nm with a shoulder peak at 333.2 nm which are attributed to the π–π^* transitions in the aromatic rings [17, 18]. Besides these peaks is a small free electro-absorption tail around 450.9 nm which can be characterized as the conductive form of PANI [18]. The absorption band around 680 nm corresponds to the intramolecular electronic transition between the quinoid and benzenoid units [19]. The PANI/CuO_{ch} and PANI/CuO_{gr} exhibit two absorption bands

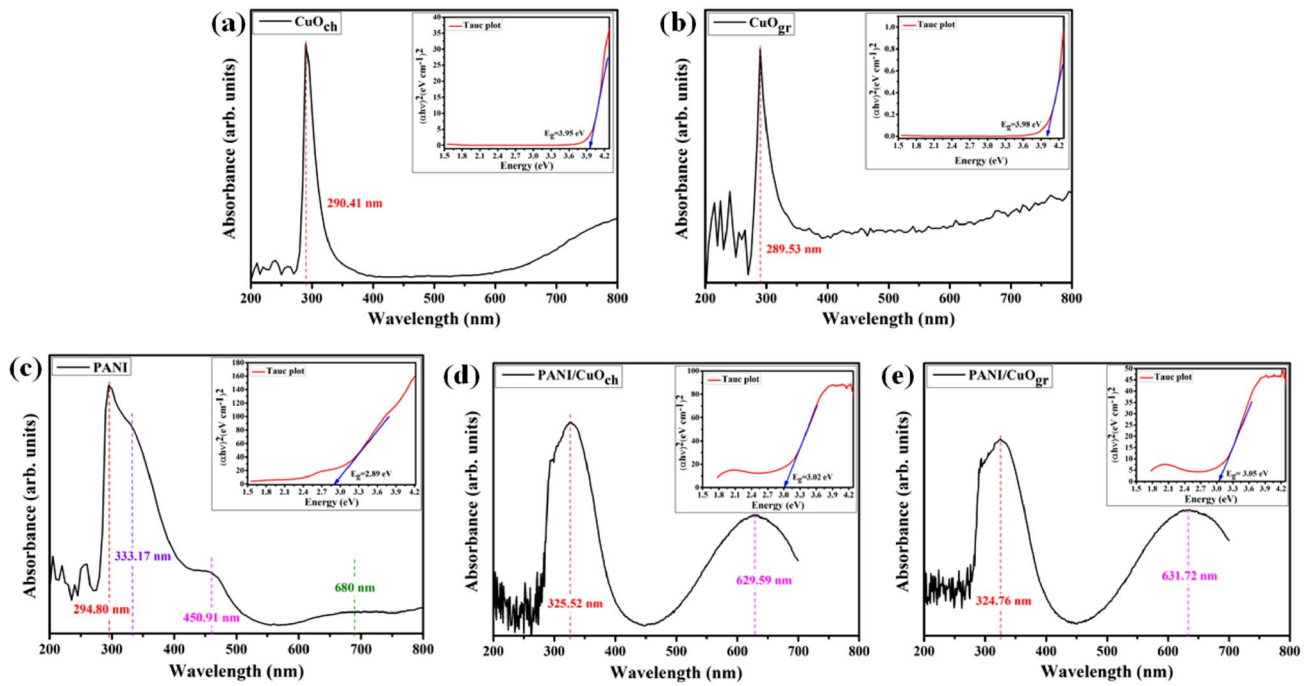

Fig. 1 UV spectra of **a** CuO_{ch}, **b** CuO_{gr}, **c** PANI, **d** PANI/CuO_{ch}, and **e** PANI/CuO_{gr} nanocomposite. Inserted is the Tauc plot

around ~ 325 nm and ~ 631 nm (Fig. 1d and e) which depend on the level of doping of the CuO with the PANI. The band gap were calculated from the intercept of the tangents to the plot of $(\alpha h\nu)^2$ vs photon energy ($h\nu$) for CuO_{ch}, CuO_{gr}, PANI, PANI/CuO_{ch}, and PANI/CuO_{gr} nanocomposite were 3.95 eV, 3.98 eV, 2.89 eV, 3.02 eV, and 3.05 eV, respectively. The results show that doping of the CuO with PANI helps in reducing band gap compared to the pristine CuO_{ch} and CuO_{gr} nanoparticles.

3.2 XRD analysis

The X-ray diffraction (XRD) analyses of the prepared CuO nanoparticle by two different methods (i.e., chemical and green synthesis methods) and their corresponding composite prepared by doping the nanoparticles with PANI were carried out for the samples phase and crystal structure identification. Figure 2a and b show the phase characteristics of CuO_{ch} and CuO_{gr} samples prepared by chemical and green synthesis routes. The diffraction peaks at 32.6°, 35.6°, 38.9°, 48.8°, 53.6°, 58.4°, 61.7°, 66.3°, 68.1°, 72.5°, 75.2°, and 83.2° can be indexed to the (110), (11–1), (111), (20–2), (020), (202), (11–3), (31–1), (220), (311), (22–2), and (222) monoclinic CuO lattice planes, respectively (JCPDS card No. 05–0661). In addition, the peak at approximately 29.5° corresponds to the Cu_2O (011) lattice plane observed for both synthesis routes, which is an indication of the presence of an impure phase within samples. As seen in Fig. 2a and b, the peak intensity of the impure phase (011) is low in the green synthesis (CuO_{gr}) as compared to the CuO synthesis through a chemical route (CuO_{ch}). This implies that the CuO synthesis through a green synthesis route contains a less impure phase. The average crystallite size calculated using the Debye–Scherrer formula [12] was found to be 13.45 nm and 15.70 nm for CuO_{ch} and CuO_{gr}, respectively. Figure 2c shows the diffraction pattern of the PANI with a main characteristic peak of the PANI crystalline orthorhombic structure at $2\theta = 24.8°$, corresponding to the basal plane (200) [20]. After doping of the CuO_{ch} and CuO_{gr} nanoparticles, the composite maintain most of the peaks observed in Fig. 2a and b with little peak shift toward the high diffraction angle, which can probably be attributed to the strong binding of the PANI into the CuO lattice matrix.

3.3 FTIR analysis

Figure 3 shows the FTIR spectra of CuO_{ch}, CuO_{gr}, PANI, PANI/CuO_{ch}, and PANI/CuO_{gr} nanocomposite. In Fig. 3a and b, the bands at ~ 490 cm^{-1} (CuO_{ch}) and ~ 494 cm^{-1} (CuO_{gr}) are related to the stretching vibration of the Cu–O bond in monoclinic CuO [21]. The peaks around 600–1000 cm^{-1} (at ~ 616 cm^{-1} and ~ 875 cm^{-1} for CuO_{ch} and ~ 871 cm^{-1} for CuO_{gr}) are attributed to the Cu–O stretching of CuO [22]. The absorption peaks at ~ 1429 cm^{-1} (CuO_{ch}) and ~ 1423 cm^{-1} (CuO_{gr}) are the stretching vibrations of the carboxylate ion group present

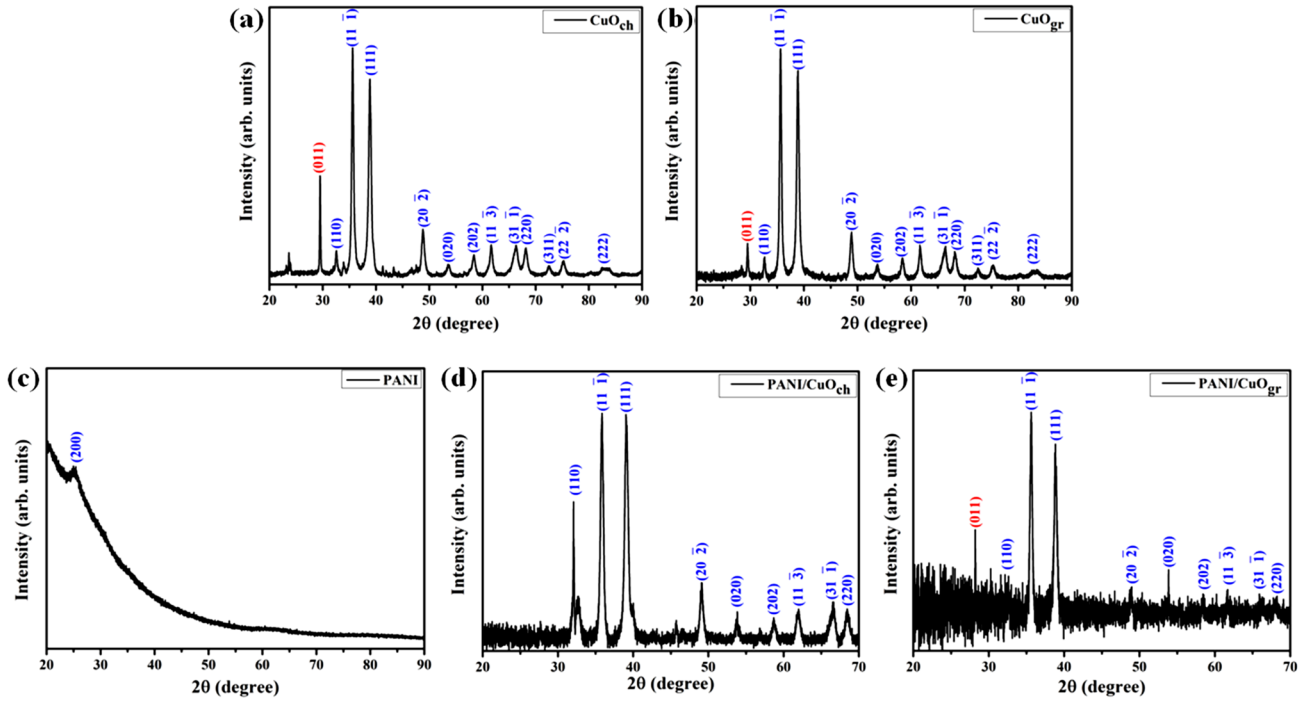

Fig. 2 XRD patterns of **a** CuO_{ch}, **b** CuO_{gr}, **c** PANI, **d** PANI/CuO_{ch}, and **e** PANI/CuO_{gr} nanocomposite

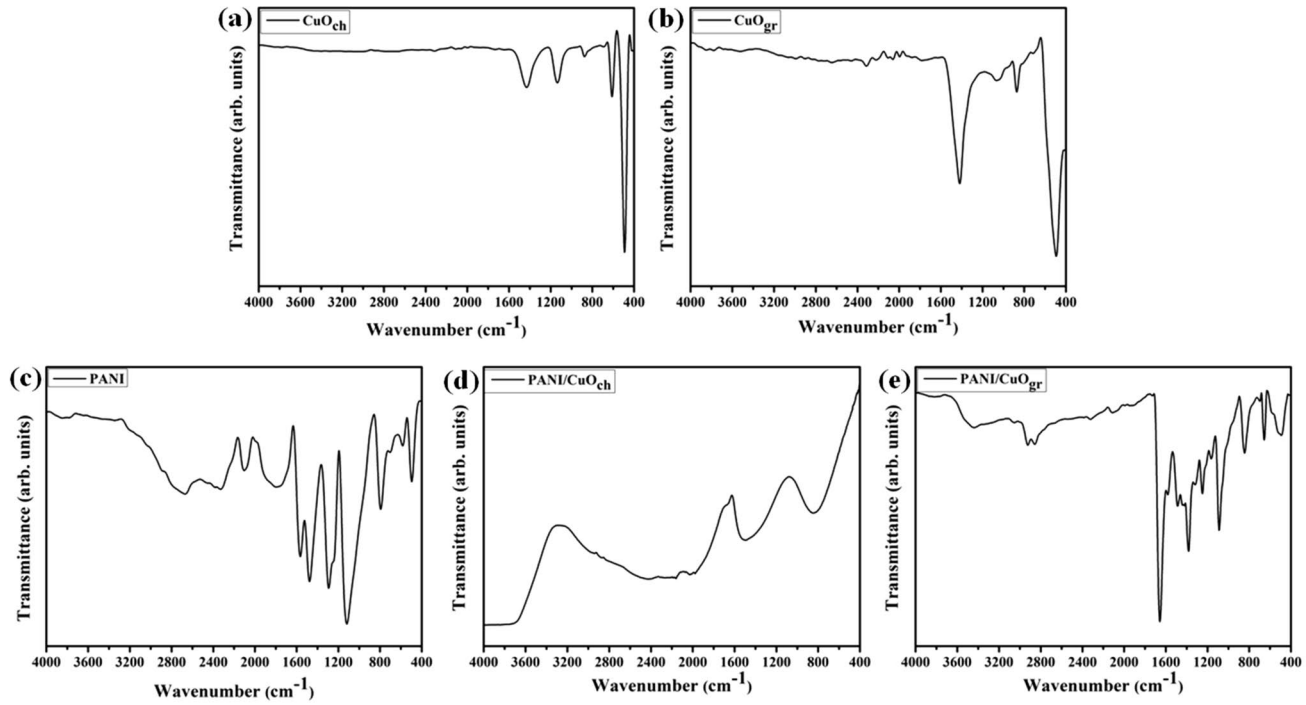

Fig. 3 FTIR spectra of **a** CuO_{ch}, **b** CuO_{gr}, **c** PANI, **d** PANI/CuO_{ch}, and **e** PANI/CuO_{gr} nanocomposite

in the ethylene glycol [23]. Bands at ~ 1136 cm^{-1} (CuO_{ch}) and ~ 1060 cm^{-1} (CuO_{gr}) show the presence of C-N stretching in primary amine and water-soluble -C–O–C- or -C-O- bonds [24]. The FTIR bands of the PANI in Fig. 3c show detected bands as ~ 3840 cm^{-1} and ~ 3444 cm^{-1} show the presence of N–H stretching [25]. While the observed peaks at ~ 2668 cm^{-1}, ~ 2331 cm^{-1}, and ~ 2102 cm^{-1} are due to irregular C-H stretching of the aromatic ring in the PANI [26]. The peaks associated with the C = C stretching in aromatic nuclei are seen at the absorption peak at ~ 1791 cm^{-1}, ~ 1567 cm^{-1}, and ~ 1472 cm^{-1} [27]. The absorption bands at ~ 1293 cm^{-1} and ~ 1122 cm^{-1} reveal the presence of the C-H bending vibrations [27, 28]. The intense bands less than 1000 cm^{-1} can be assigned to the out-of-plane bending mode of aromatic C-H groups [29]. However, the peak patterns in Fig. 3d and e for PANI/CuO_{ch}, and PANI/CuO_{gr}, respectively, show that when the CuO is doped with PANI, combined absorption peaks of the CuO and PANI were observed, which is an indication of the binding between the PANI and the nanoparticles. The observed peaks associated with bending and stretching vibrations of adsorbed water and surface hydroxyl groups in the PANI/CuO_{ch}, and PANI/CuO_{gr} FTIR spectrum show that the prepared nanocomposites will be promising for the detection of dopamine [DA] which will be explained in Sect. 3.7.

3.4 SEM analysis

Figure 4 shows the SEM microgram of CuO_{ch}, CuO_{gr}, PANI, PANI/CuO_{ch}, and PANI/CuO_{gr} nanocomposite. The SEM image of CuO_{ch} (Fig. 4a) shows what looks like an agglomeration of glassy form particles. While the SEM image of CuO_{gr} (Fig. 4b) show the formation of slightly spherical agglomerated particle. The particle size of CuO_{ch} was not visible clearly due to the agglomeration being more compared to CuO_{gr}. The SEM image of the PANI in Fig. 4c shows the presence of a granular morphology with better cohesion and higher aggregation than what is observed in the case of CuO_{ch} and CuO_{gr} morphology. The average diameter of the PANI granular is in the range of yum. The SEM image of PANI/CuO_{ch} (Fig. 4d) shows a morphology with less agglomeration of the particles. While in the case of PANI/CuO_{gr}, the SEM morphology (Fig. 4e) shows that the grains are loosely packed. Therefore, it can be concluded that doping of CuO_{ch} and CuO_{gr} with PANI makes the particles less agglomerated than observed in CuO_{ch} and CuO_{gr} morphology. The EDS compositional analysis results of the materials are shown in Fig. 5, which confirmed the presence of all the expected elements.

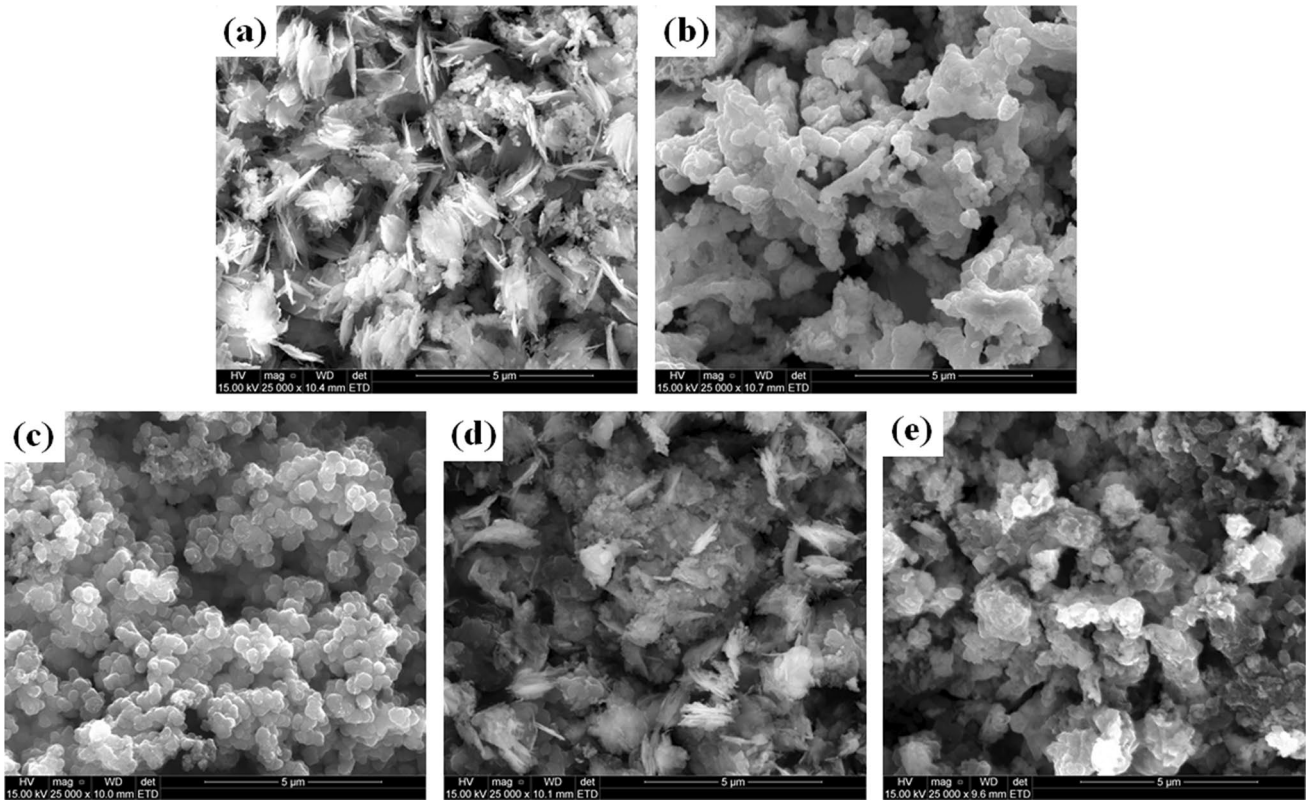

Fig. 4 SEM micrograph of **a** CuO_{ch}, **b** CuO_{gr}, **c** PANI, **d** PANI/CuO_{ch}, and **e** PANI/CuO_{gr} nanocomposite

3.5 Electrochemical measurement

Prior to the electrochemical performance of the electrodes, the optimization of the best ratio of PANI to CuO_{ch} and CuO_{gr} in the formation of the PANI/CuO_{ch}, and PANI/CuO_{gr} nanocomposites was conducted using a CV in a 5 mM $[Fe(CN)_6]^{-3/4-}$ in 0.1 phosphate buffer saline (PBS) at pH = 7.4. Figure 6 shows the CV curves for PANI/CuO_{ch}, and PANI/CuO_{gr} at different ratios starting from 1:1, 1:2, and 1:3 for the PANI to CuO. As seen in Fig. 6a and c, for both PANI/CuO_{ch} and PANI/CuO_{gr} nanocomposites, a maximum peak current was obtained for the sample at 1:1, which is an indication that the ratio of PANI to CuO plays a significant role in the electrochemical performance of an electrode. Hence one to one ratio (1:1) of PANI to CuO was chosen for further experimental studies.

The electrochemical performance of Bare, CuO_{ch}, CuO_{gr}, PANI/CuO_{ch}, and PANI/CuO_{gr} electrodes were investigated in 5 mM $[Fe(CN)_6]^{-3/4-}$ in 0.1 PBS at pH of 7.4 by sweeping the potential from − 0.5 to 0.9 V with a 25 mV/s scan rate. As seen in Fig. 7a, the voltammograms recorded in the redox system presented a pair of well-defined redox peaks of the $[Fe(CN)_6]^{-3/4-}$ redox couple probe on the five electrodes, respectively. The relatively peak current intensity from the low to high is noted to be in the order of $CuO_{ch} < CuO_{gr} <$ Bare < PANI/CuO_{ch} < PANI/CuO_{gr} (Fig. 7b). The observed highest peak current intensity on PANI/CuO_{gr} electrode is an indication that the PANI/CuO_{gr} electrode has the optimum sensitive electronic characteristics and strong adsorption capacity which can be attributed to the doping process of CuO_{gr} with PANI to give an enhanced morphology (See Fig. 4). The effective electroactive surface area (EASA) of the electrodes were evaluated in terms of the Randles–Sevcik equation from the CV [30]:

$$I_p = 2.69 \times 10^5 n^{\frac{3}{2}} A D^{\frac{1}{2}} C v^{\frac{1}{2}} \quad (1)$$

where I_p is the anodic peak current (A), n is the number of electrons transferred, A is the effective electroactive surface area (cm^2), C is the concentration of $K_3Fe(CN)_6$ (mol cm^{-3}), D is the diffusion coefficient (cm^2 s^{-1}), and v is the scan rate (v s^{-1}). The values of the calculated EASA for Bare, CuO_{ch}, CuO_{gr}, PANI/CuO_{ch}, and PANI/CuO_{gr} electrodes are 1.03, 0.73, 0.9, 1.30, and 1.31 cm^2, respectively. The value of EASA of PANI/CuO_{gr} is 45.56% and 27.18% larger than the Bare and pristine CuO_{gr} nanoparticles, respectively. This enhancement in the electrode EASA results in increased number of catalytic sites for electrochemical oxidation.

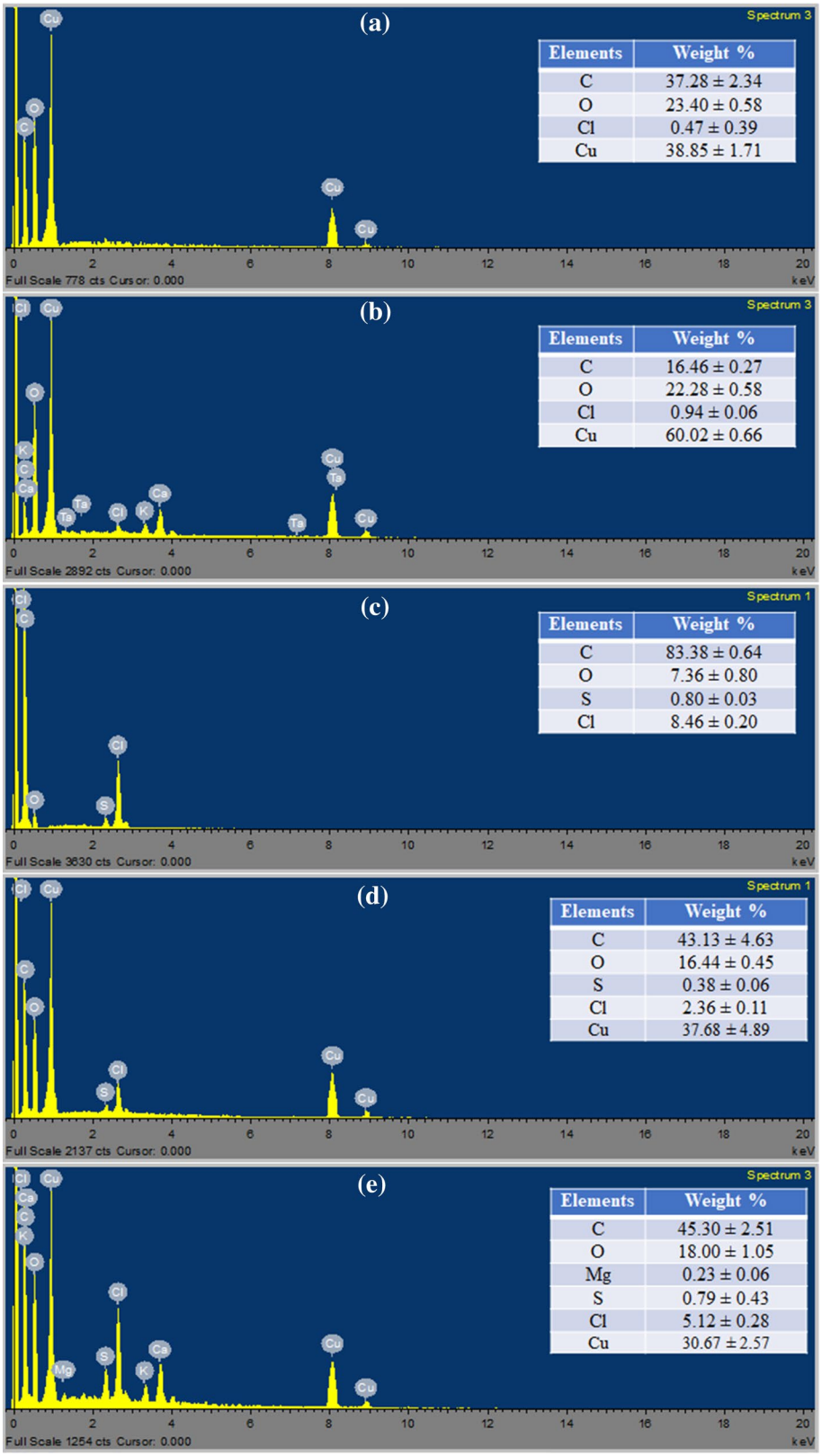

Fig. 5 EDS spectra of **a** CuO_{ch}, **b** CuO_{gr}, **c** PANI, **d** PANI/CuO_{ch}, and **e** PANI/CuO_{gr} nanocomposite

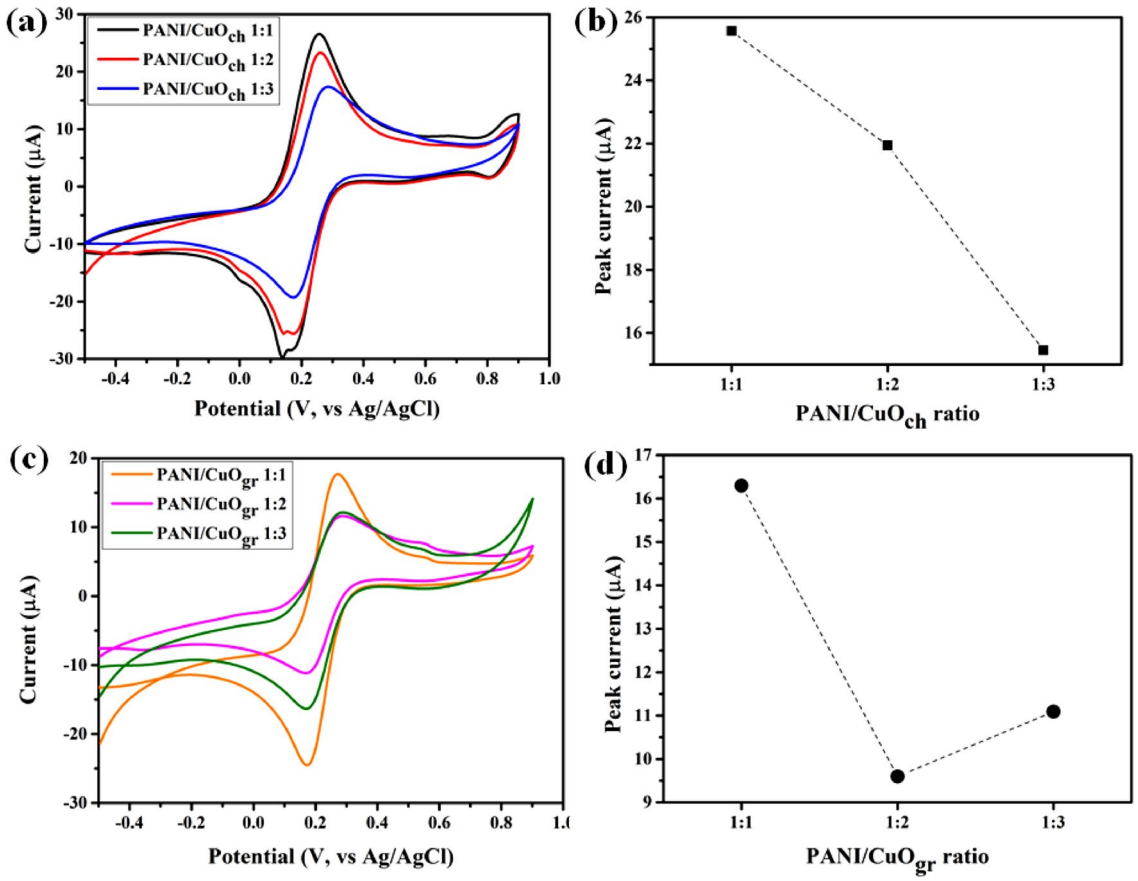

Fig. 6 Cyclic voltammogram of optimization between **a** PANI to CuO_{ch} ratio, **b** anodic current response of PANI to CuO_{ch} ratio, **c** PANI to CuO_{gr} ratio, **d** anodic current response of PANI to CuO_{gr} ratio

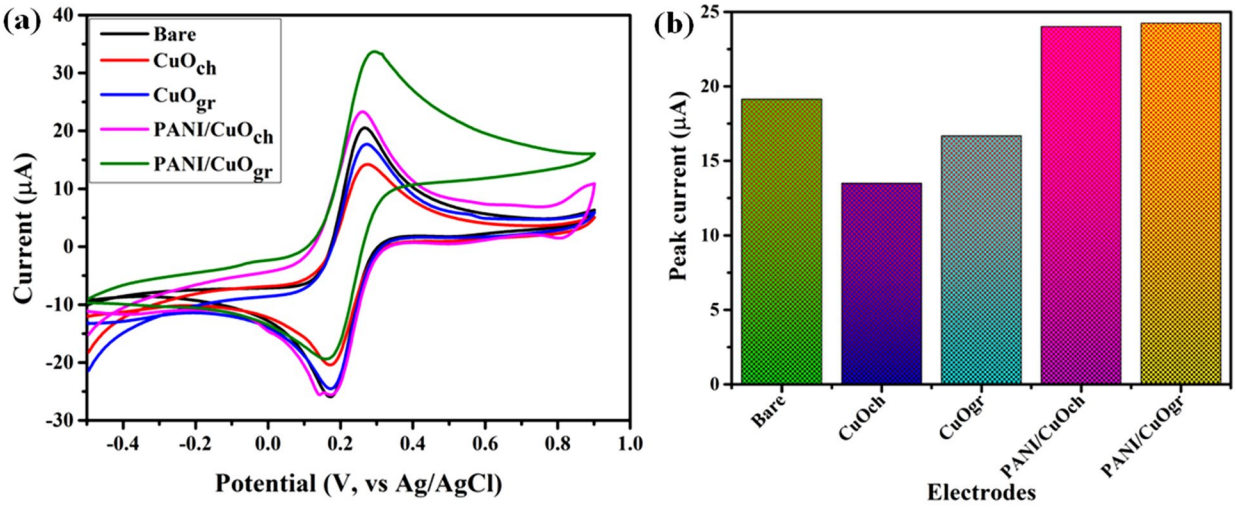

Fig. 7 **a** Cyclic voltammogram **b** anodic current response of Bare, CuO_{ch}, CuO_{gr}, PANI/CuO_{ch}, and PANI/CuO_{gr} nanocomposite

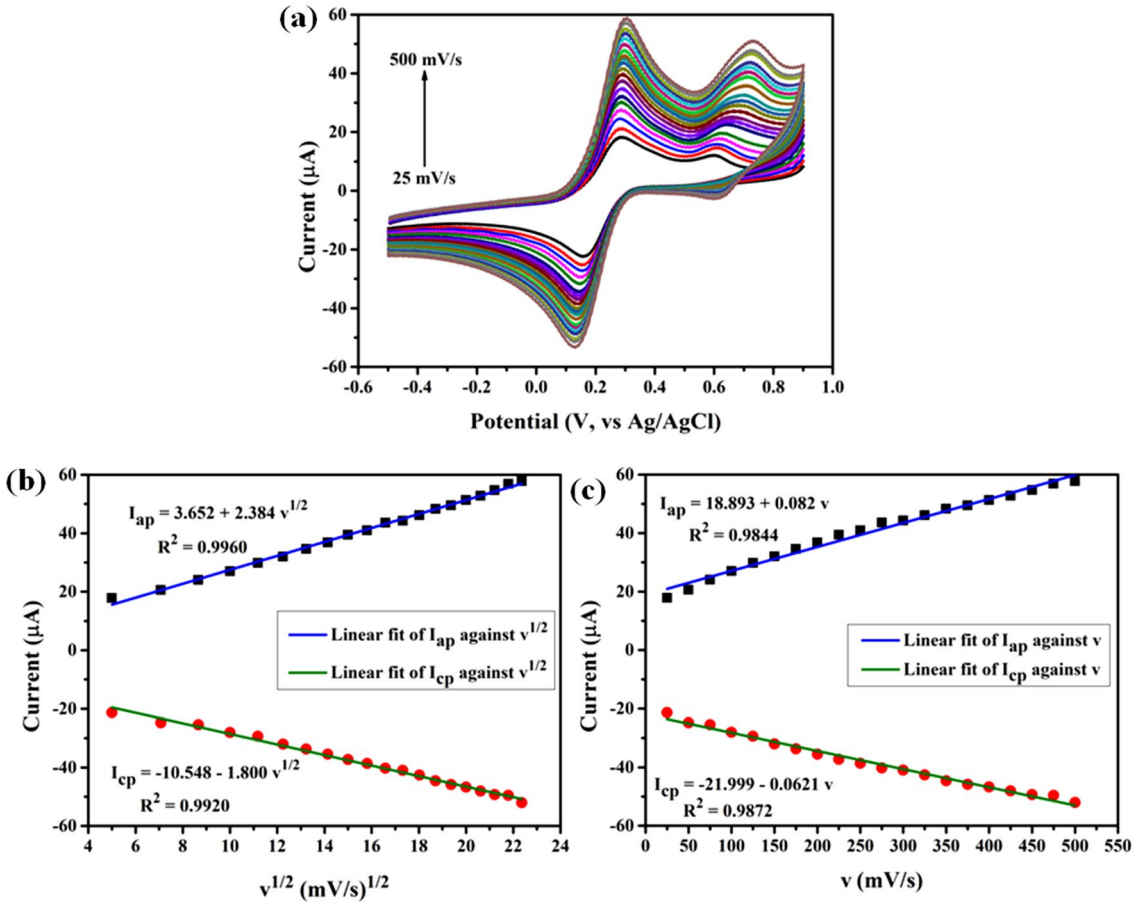

Fig. 8 **a** Cyclic voltammetric response toward $[Fe(CN)_6]^{-3/4-}$ on PANI/CuO_{ch} electrode at different scan rates ranging from 25 mV/s to 500 mV/s, **b** plot of current vs square root of scan rate, and **c** plot of current vs scan rate

3.6 Effect of scan rate

The effect of scan rate on the peak current and peak potential of 5 mM $[Fe(CN)_6]^{-3/4-}$ in 0.1 phosphate buffer saline (PBS) (pH = 7.4) at the PANI/CuO_{ch} and PANI/CuO_{gr} electrodes was studied by cv. In this analysis, PANI/CuO_{ch}, and PANI/CuO_{gr} electrodes were chosen because they give a better anodic current response and optimum EASA value compared to Bare, CuO_{ch}, and CuO_{gr} nanoparticles (See Fig. 7). Figures 8a and 9a show the CV responses on PANI/CuO_{ch} and PANI/CuO_{gr} electrodes at scan rates ranging from 25 mV/s to 500 mV/s. The peak current in both the two electrodes increases with an increase in the scan rate and satisfactory linearity was obtained from the plots of i_p versus square root of the scan rate (Figs. 8b and 9b) and scan rate (Figs. 8c and 9c), respectively. The corresponding linear regression equation is expressed as follows:

For PANI/CuO_{ch} electrodes

$$I_{ap}(\mu A) = 3.652 + 2.384v^{\frac{1}{2}} \ (R^2 = 0.9960) \quad (2a)$$

$$I_{ap}(\mu A) = 18.893 + 0.082v \ (R^2 = 0.9844) \quad (2b)$$

$$I_{cp}(\mu A) = -10.548 - 1.800v^{\frac{1}{2}} \ (R^2 = 0.9920) \quad (3a)$$

$$I_{cp}(\mu A) = -21.999 - 0.0621v \ (R^2 = 0.9872) \quad (3b)$$

For PANI/CuO_{gr} electrodes

$$I_{ap}(\mu A) = 11.549 + 2.245v^{\frac{1}{2}} \ (R^2 = 0.9817) \quad (4a)$$

$$I_{ap}(\mu A) = 25.6783 + 0.078v \ (R^2 = 0.9927) \quad (4b)$$

$$I_{cp}(\mu A) = -19.609 - 1.667v^{\frac{1}{2}} \ (R^2 = 0.9848) \quad (5a)$$

$$I_{cp}(\mu A) = -30.178 - 0.058v \ (R^2 = 0.9855) \quad (5b)$$

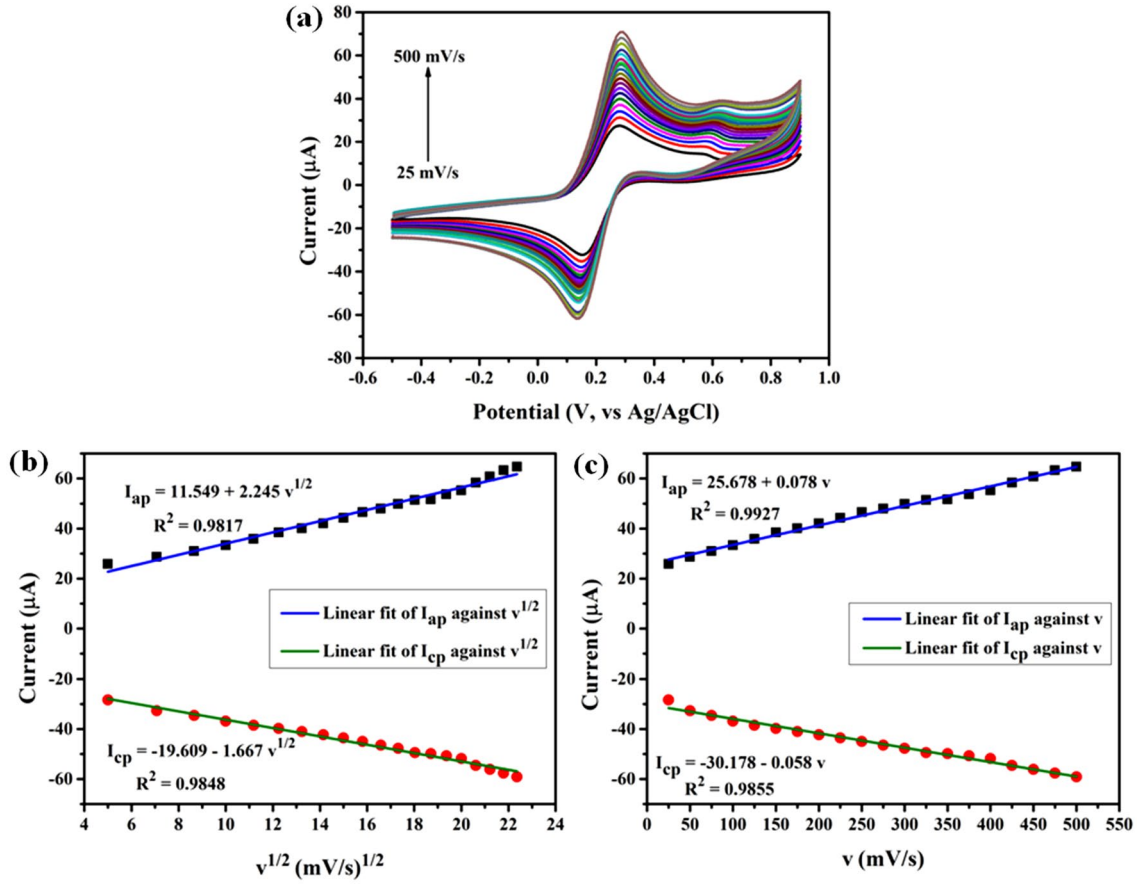

Fig. 9 **a** Cyclic voltammetric response toward $[Fe(CN)_6]^{-3/4-}$ on PANI/CuO_{gr} electrode at different scan rates ranging from 25 mV/s to 500 mV/s, **b** plot of current vs square root of scan rate, and **c** plot of current vs scan rate

The above observation predicts that the oxidation of $[Fe(CN)_6]^{-3/4-}$ is adsorption controlled at the surface of PANI/CuO_{ch}, and PANI/CuO_{gr} electrodes.

3.7 Dopamine (DA) detection

The electrochemical behavior of PANI/CuO_{ch} and PANI/CuO_{gr} electrodes toward dopamine (DA) was investigated using CV at scan rates ranging from 25 to 500 mV/s in the presence of DA in a PBS buffer of pH 7.4. As shown in Fig. 10a, the anodic/cathodic peak current increases with an increase in the scan rate. While the plot of the oxidation peak current against the square root of the scan rate ($v^{1/2}$) (Fig. 10b) shows a linear relationship with the $v^{1/2}$ as fitted by $I_{ap}(\mu A) = -36.560 + 12.690v^{\frac{1}{2}}$ $(R^2 = 0.9850)$ and $I_{cp}(\mu A) = 23.088 - 19.919v^{\frac{1}{2}}$ $(R^2 = 0.9433)$ for PANI/CuO_{ch} Moreover, similar observations were seen for PANI/CuO_{gr} electrode (Fig. 11a) with fitted equation $I_{ap}(\mu A) = 28.644 + 2.159v^{\frac{1}{2}}$ $(R^2 = 0.9546)$ and $I_{cp}(\mu A) = 3.376 - 1.980v^{\frac{1}{2}}$ $(R^2 = 0.9577)$ (Fig. 11b). These results suggest that the oxidation of DA is adsorption controlled at the surfaces of both PANI/CuO_{ch} and PANI/CuO_{gr} electrodes, respectively [31, 32]. Furthermore, the influence of scan rate on the redox peak potential was investigated. With an increase in the scan rate, the oxidation and reduction peak potentials shift slightly to the right and left direction, respectively. Hence, the electron transfer kinetic parameters, such as the electron transfer coefficient (α) and the number of electron transfers (n) of DA on PANI/CuO_{ch} and PANI/CuO_{gr} were estimated using Laviron's equation [33, 34]:

$$E_{ap} = E^o + \frac{2.303RT}{(1-\alpha)nF}\log(v) \tag{6}$$

$$E_{cp} = E^o - \frac{2.303RT}{\alpha nF}\log(v) \tag{7}$$

where E^o is the formal potential, n is the number of electrons transferred, α is the electron transfer coefficient, R is the gas constant ($R = 8.314$ J K^{-1} mol^{-1}), T is the temperature (298 K), and F is the faraday constant (96,500 C mol^{-1}).

The linear relationships between the oxidation and reduction peaks potentials (E_{ap} and E_{cp}) versus the logarithm of scan rate (ν) (log ν) are presented in Figs. 10d and

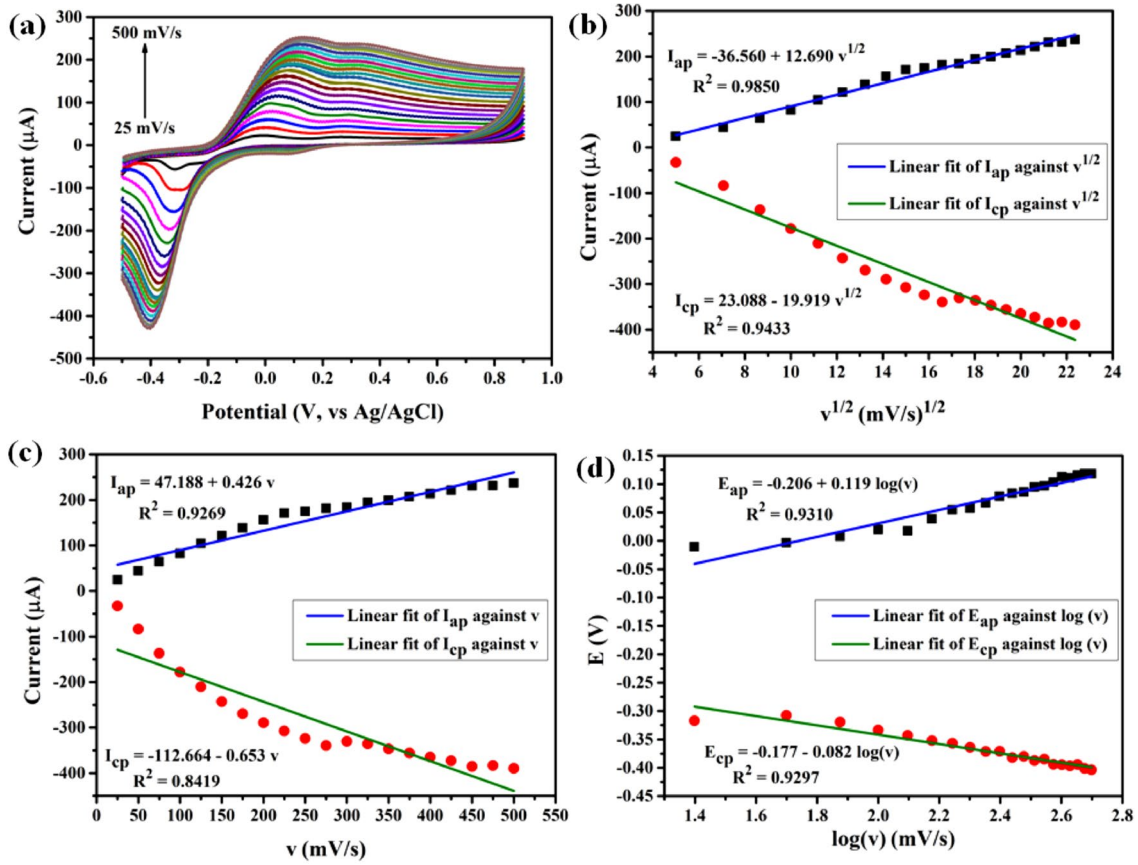

Fig. 10 **a** Cyclic voltammetric response toward DA on PANI/CuO_{ch} electrode at different scan rates ranging from 25 to 500 mV/s, **b** plot of current vs square root of scan rate, **c** plot of current vs scan rate, and **d** plot of peak potential vs log (v)

11d. The corresponding regression equation is: $E_{ap}(V) = -0.206 + 0.119\log(v)(R^2 = 0.9310)$ and $E_{cp}(V) = -0.177 - 0.082\log(v)(R^2 = 0.9577)$ for PANI/CuO_{ch} electrode and $E_{ap}(V) = -0.075 + 0.045\log(v)(R^2 = 0.9276)$ and $E_{cp}(V) = -0.342 - 0.011\log(v)(R^2 = 0.2398)$ for PANI/CuO_{gr} electrode. According to Laviron's equation (Eq. (6) and (7)), the slopes are equal to $\frac{2.303RT}{(1-\alpha)nF}$ and $-\frac{2.303RT}{\alpha nF}$ for the anodic and cathodic peaks, respectively. Thus, the number of electrons transferred (n) and electron transferred coefficient (α) were calculated to be 0.721 (~1) and 0.592 for PANI/CuO_{ch} electrode and 5.375.721 (~5) and 0.804 for PANI/CuO_{gr} electrode, respectively. The relatively higher value of n and α show that PANI/CuO_{gr} nanocomposite can effectively enhance the electron transfer between the electrode surface and DA.

In addition, the adsorption capacity of the DA at PANI/CuO_{ch} and PANI/CuO_{gr} surface were also calculated using the equation [34]:

$$i_p = \frac{n^2F^2}{4RT}\Gamma A\nu \tag{8}$$

where Γ is the adsorption capacity (mol cm^{-2}), and ν, n, F, R, T, and A are as described in Eqs. (1), (5), (7). Therefore, the surface coverage of the DA at the PANI/CuO_{ch} and PANI/CuO_{gr} was calculated to be 6.709×10^{-7} mol/cm^2 and 2.053×10^{-9} mol/cm^2, respectively.

3.8 Electroanalysis of DA

Square wave voltammetry (SWV) was used in the electroanalysis of dopamine on the nanocomposite electrodes because of the better sensitivity of the SWV than the CV [1]. Therefore, the SWV was used to investigate the effect of concentration ranging from 26 to 95 μM in PBS (pH = 7.4) on the electrode's response to DA oxidation. For PANI/CuO_{ch} electrode, an increase in the current response was observed with an increase in the DA

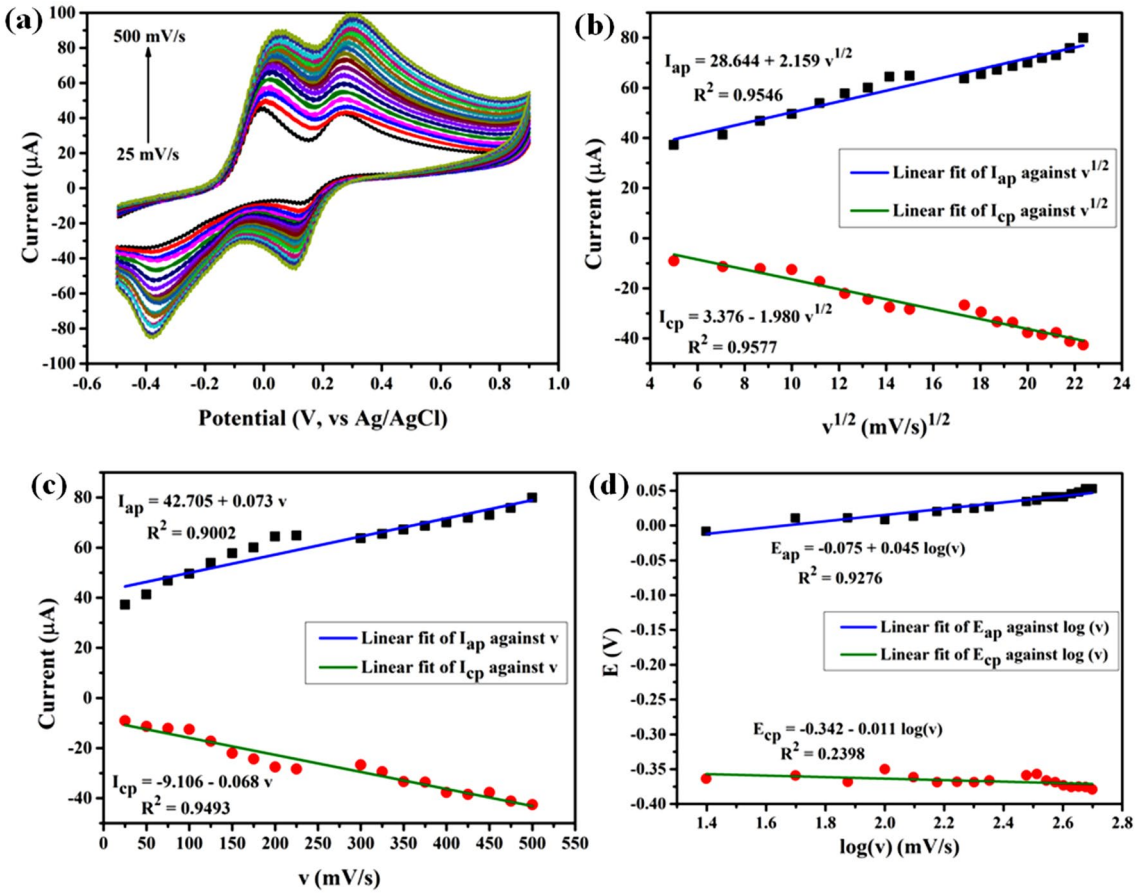

Fig. 11 **a** Cyclic voltammetric response toward DA on PANI/CuO_{gr} electrode at different scan rates ranging from 25 to 500 mV/s, **b** plot of current vs square root of scan rate, **c** plot of current vs scan rate, and **d** plot of peak potential vs log (*v*)

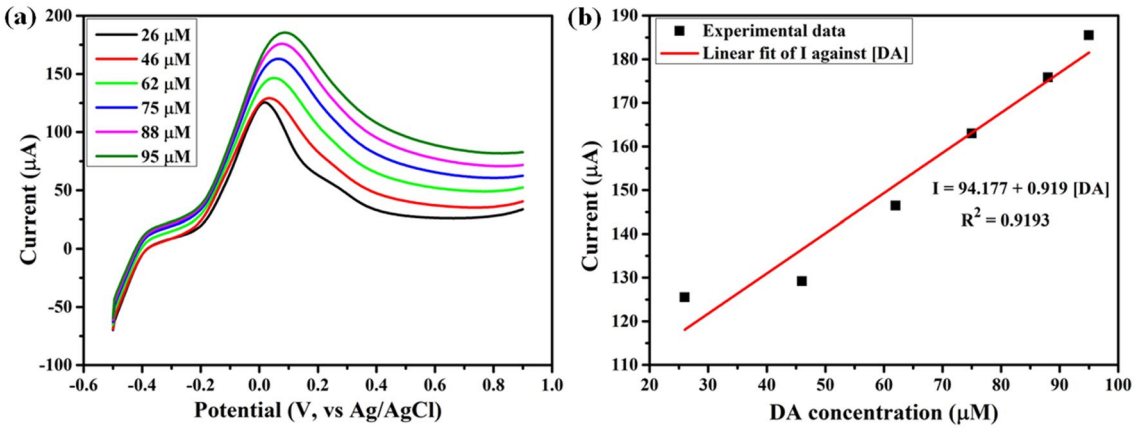

Fig. 12 **a** SWV voltammograms of different concentrations of DA on PANI/CuO_{ch} electrode (**b**) plot of peak current as a function of the concentration of DA

concentration (Fig. 12a). While the plot of the concentration over the range from 26 μM to 95 μM against the current response in Fig. 12b gave a linear relationship $I(\mu A) = 94.177 + 0.919[\mathrm{DA}]\left(R^2 = 0.9193\right)$. On the other hand, for PANI/CuO_{gr} electrode, the current response

decreases with an increase in the DA concentration from 26 to 95 µM (Fig. 13a). While the corresponding plot of its concentration against the current response shows a better linear relationship: $I(\mu A) = 79.176 - 0.388[\mathrm{DA}]\left(R^2 = 0.9938\right)$. Based on the correlation coefficient, the DA oxidation on PANI/CuO_{gr} electrode shows a better linear relationship between the peak current and the analyte concentration than PANI/CuO_{ch} electrode. Furthermore, based on the results from the SWV techniques, the limits of detection (LOD) ($LOD(\mu M) = 3.3\frac{\delta}{m}$) are estimated using the relationship between the relative standard deviation of the intercept (δ) and the slope (m) of the linear relationship in Figs. 12b and

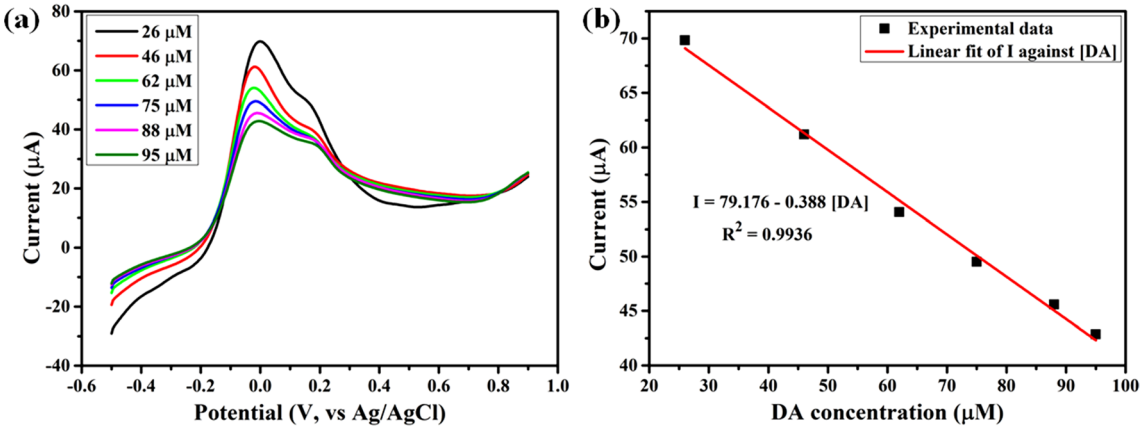

Fig. 13 **a** SWV voltammograms of different concentrations of DA on PANI/CuO_{gr} electrode (**b**) plot of peak current as a function of the concentration of DA

Table 1 Comparison of previous sensors' results with the present study

Electrodes	LOD (µM)	Linear range (µM)	Technique	References
CQDs/CuO	25.40	10–180	SWV	[30]
PANI-NF/Pt	33.30	62.5–603	SWV	[35]
rGO/AuNPs	20	1–60	DPV	[36]
AuNPs/DNA/o–PD/SPCE	1000	–	CV	[37]
Nano-Au/SAMs gold	90	200–1200	DPV	[38]
PANI/CuO_{ch}	25.90	26–95	SWV	**This work**
PANI/CuO_{gr}	8.22	26–95	SWV	**This work**

The bold is to just indicate the important parameters considered

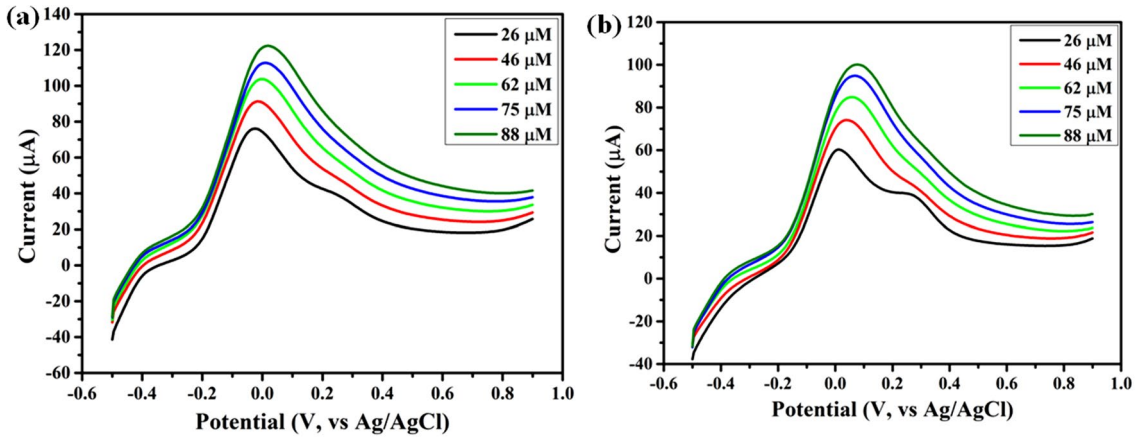

Fig. 14 **a** SWV voltammograms by keeping the AA concentration constant at 1 mM with an increase in DA concentration from 26 to 88 µM on **a** PANI/CuO_{gr} and **b** PANI/CuO_{gr} electrodes

13b. The LOD is estimated to be 25.90 and 8.22 µM for PANI/CuO_{ch} and PANI/CuO_{gr} electrodes, respectively. This result indicates that PANI/CuO_{gr} electrode has high sensitivity and low detection limit than the PANI/CuO_{ch} electrode, which implies that the synthesis route of the nanocomposites plays a significant role in its electroactive properties. A comparison between the electrodes in this study and other modified electrodes toward detection of DA is presented in Table 1 and the results obtained for both PANI/CuO_{ch} and PANI/CuO_{gr} electrodes are comparable with the reported literature results [30, 35–38].

3.9 Interference studies

The interference study was carried out with the adoption of ascorbic acid (AA) as the interfering substance with DA. Figure 14 shows the result from the interference experiment which is obtained by keeping the AA concentration constant at 1 mM with an increase in DA concentration from 26 to 88 µM. It is evident from Fig. 14a and b that the current response of the DA increases with an increase in the DA concentrations for PANI/CuO_{ch} and PANI/CuO_{gr} electrodes, respectively. Although, at a lower DA concentration of 26 µM, the AA peak was observed which tends to outrightly disappear at the higher DA concentration (i.e., 62 to 88 µM). This phenomenon is a clear indication that the modified electrodes in this study might be highly selective for DA determination. The selectivity of DA toward PANI/CuO_{ch}, and PANI/CuO_{gr} electrodes at pH of 7.4 might be attributed to the presence oxygen-containing functional group on the electrode as observed from the FTIR spectrum in Fig. 3e, which can attract the positively charged on the DA. Also, the increase in the DA concentration can lead to a reduction in the chances of AA oxidation which might favor the detection of the DA on the electrodes.

4 Conclusions

In this study, CuO nanoparticles were synthesized using two different routes: chemical and green synthesis. The prepared CuO (i.e., CuO_{ch} and CuO_{gr}) were successfully doped with PANI to enhance their electrochemical properties. The novel PANI/CuO_{ch} and PANI/CuO_{gr} have the advantages of high current response, a low detection limit, and good selectivity for DA. This result indicates that PANI/CuO_{gr} electrode has high sensitivity and low detection limit than the PANI/CuO_{ch} electrode, which implies that the synthesis route of the nanocomposites plays a significant role in its electroactive properties.

Acknowledgements CEO, SAA, and OEF thank the North-West University and MaSIM for their financial support and research facilities. OEF acknowledges the FRC of North-West University and the National Research Foundation of South Africa for Thuthuka funding for Researchers (UID: 117709).

Author contributions OEF conceptualized and designed the work and was part of the manuscript write-up. SJK, and AA was involved in the manuscript preparation. All the authors reviewed the manuscript and agreed to publication.

Funding Open access funding provided by North-West University. This research was funded by the National Research Foundation of South Africa for Thuthuka funding for Researchers (UID: 117709).

Data availability The data for this study will be made available only upon request from the corresponding author.

Declarations

Conflict of interest The authors declare no conflict of interest.

References

1. H. Li, K. Zhou, J. Cao, Q. Wei, C.T. Lin, S.E. Pei, L. Ma, N. Hu, Y. Guo, Z. Deng, Z. Yu, S. Zeng, W. Yang, L. Meng, Carbon **171**, 16–28 (2021)
2. J.G. Nutt, G.F. Wooten, N. Engl, J. Med. **353**, 1021–1027 (2005)
3. K. Chaiendoo, S. Ittisanronnachai, V. Promarak, W. Ngeontae, Carbon **146**, 728–735 (2019)
4. R.M. Wightman, L.J. May, A.C. Michael, Anal. Chem. **60**, 769A-779A (1988)
5. R.D. Badgaiyan, Front. Neurosci. **7**, 125 (2013)
6. B.B. Anderson, A.G. Ewing, J. Pharmaceut. Biomed. Anal. **19**, 15–32 (1999)
7. J.F. van Staden, R.I.S. van Staden, Talanta **102**, 34–43 (2012)
8. A. Suzuki, T.A. Ivandini, K. Yoshimi, A. Fujishima, G. Oyama, T. Nakazato, N. Hattori, S. Kitazawa, Y. Einaga, Anal. Chem. **79**, 8608–8615 (2007)
9. W. Cai, J. Lai, T. Lai, H. Xie, J. Ye, Sens. Actuators B-Chem. **224**, 225–232 (2016)
10. V.K. Jha, Nep. J. Integr. Sci. **2**, 42–46 (2012)
11. O.E. Fayemi, O.G. Pooe, F.A. Adesanya, I.P. Ejidike, Nanomater. **12**, 1825 (2022)
12. B. Uma, K.S. Anantharaju, L. Renuka, S. Malini, S.S. More, Y.S. Vidya, S. Meena, Ceram. Int. **47**, 10355–10369 (2021)
13. X. Huang, H. Wu, S. Pu, W. Zhang, X. Liao, B. Shi, Green Chem. **13**, 950 (2011)
14. Z. Wang, C. Fang, M. Megharaj, A.C.S. Sustain, Chem. Eng. **2**, 1022 (2014)

15. E.C. Okpara, O.E. Fayemi, E.M. Sherif, P.S. Ganesh, B.E.K. Swamy, E.E. Ebenso, Sens. Bio-Sens. Res. **35**, 100476 (2022)
16. K.R. Shubhashree, R. Reddy, A.K. Gangula, G.S. Nagananda, P.K. Badiya, S.S. Ramamurthy, P. Aramwit, N. Reddy, Mater. Chem. Phys. **280**, 125795 (2022)
17. A.B. Samui, A.S. Patanakar, R.S. Satpute, P.C. Deb, Synth. Met. **125**, 423–427 (2002)
18. D.C. Sindhimeshram, M.C. Gupta, Indian J. Chem. **34A**, 260–277 (1995)
19. Q. Qin, Y. Guo, J. Nanomater. **1**, 6 (2012)
20. Q. Jia, S. Shan, L. Jiang, Y. Wang, D. Li, J. Appl. Poly. Sci. **125**, 3560–3566 (2012)
21. R.A. Nyquist, R.O. Kagel, *Infrared Spectra of Inorganic Compounds*, 1st edn. (Academic Press, New York, 1971) p. 220
22. M. Abdelaziz, E.M. Abdelrazek, M. Phys. B **390**, 1–7 (2007)
23. S.S. Shankar, A. Ahmad, M. Sastry, Biotechnol. Prog. **19**, 1627–1631 (2003)
24. V.K. Patel, S. Bhattacharya, A.C.S. Appl, Mater. Interfaces **5**, 13364–13374 (2013)
25. F. Kanwal, S.A. Siddiqi, S. Tasleem, J. Chem. Soc. Pak. **31**, 882–887 (2009)
26. S.M. Reda, S.M. Al-Ghannam, Adv. mater. Phys. Chem. **2**, 75 (2012)
27. J. Vivekanandan, V. Ponnusamy, A. Mahudeswaran, P.S. Vijayanand, Arch. Appl. Sci. Res. **3**, 147–153 (2011)
28. H.R. Humud, T.K. Aubais, Phys. Sci. Res. Int. **5**, 110–122 (2013)
29. L. Zhang, Electrochim. Acta **52**, 6969–6975 (2007)
30. S.E. Elugoke, O.E. Fayemi, A.S. Adekunle, B.B. Mamba, T.T.I. Nkambule, E.E. Ebenso, FlatChem **33**, 100372 (2022)
31. J. Ping, J. Wu, Y. Wang, Y. Ying, Biosens. Bioelectron. **34**, 70–76 (2012)
32. Y.J. Yang, Sens. Actuators B Chem. **221**, 750–759 (2015)
33. E. Laviron, J. Electroanal. Chem. **52**, 355–393 (1974)
34. E. Laviron, J. Electroanal. Chem. **101**, 19–28 (1979)
35. H. Yu, Y. Pang, J. Tang, Int. J. Electrochem. Sci. **10**, 8353–8360 (2015)
36. S. Liu, J. Yan, G.W. He, D.D. Zhong, J.X. Chen, L.Y. Shi, X.M. Zhou, H.J. Jiang, J. Electroanal. Chem. **672**, 40–44 (2012)
37. M. Ouellette, J. Mathault, S.D. Niyonambaza, A. Miled, E. Boisselier, Coatings **9**, 496 (2019)
38. J.B. Raoof, A. Kiani, R. Ojani, R. Valiollahi, S. Rashid-Nadimi, J. Solid State Electrochem. **14**, 1171–1176 (2010)